A Discrimination Analysis of Sloan and Johnson Photometric Systems for Non-Resolved Object Characterization

Tamara E. Payne, Philip J. Castro
Applied Optimization Inc.
Joseph W. Moody
Brigham Young University
Elizabeth A. Beecher
Air Force Research Laboratory/RYWW
Matthew D. Fisher, Roberto I. Acosta
NASIC/GSMS

ABSTRACT

Accurate calibrations are critical to the ability to extract reliable features from the photometry such as albedo-Area and for fusion of data taken with different sensors. The new large stellar calibration catalogs produced by astronomers can be leveraged to improve the photometric calibrations of Resident Space Objects (RSOs). These catalogs use the Sloan filter set. In order to utilize these new catalogs, we need to evaluate the satellite discrimination capability of this filter set. Past research has shown that photometry taken in the Johnson-Cousins filter set and specialized filter sets such as SILC makes it possible to classify geosynchronous satellites by their bus type and uniquely identify them. In this work, we collect photometric signatures on a selected set of geosynchronous satellites in both Sloan and Johnson. With these measurements we compute the color indices and use the Mahalanobis distance as a metric of discrimination. We perform a statistical analysis on the metric to quantify the discrimination capability of each filter set.

1. INTRODUCTION

Sensor time is precious for collecting space object brightness measurements, especially under photometric conditions. These conditions are loosely defined as no visible clouds with sky transparency variations under 2%. The latter can only be assessed through analysis of photometric standard stars.[1] Taking the time to take calibration star data at the expense of continued collections on Resident Space Objects (RSOs) is therefore undesirable. However, well-calibrated RSO brightness measurements put on a standard system (so that measurements from different sensors at different sites can be merged together) is highly desirable. Therefore, the SSA community as a whole would benefit from the ability to perform in-frame photometric calibrations that ideally remove, but certainly reduce the need to collect calibration star data separately from RSO data.

The goal of achieving in-frame calibrations has become more nearly attainable by switching to the Sloan photometric system. The astronomical community is tending to replace the Johnson filters with the Sloan filters [1] as the primary photometric system for optical observations. The most recent large astronomical surveys in the optical regime use the Sloan filters, beginning with the Sloan Digital Sky Survey (SDSS) [2] [3] that introduced the Sloan photometric system [1], and most recently with the Panoramic Survey Telescope and Rapid Response System (Pan-STARRS) [4] [5]. Both of these surveys use what is generally referred to as the Sloan photometric system, although individual differences exist between the filters used by SDSS and those used by Pan-STARRS [4].
Unfortunately, switching to the Sloan filters is not without problems in that it has not yet been demonstrated that the Sloan system provides good satellite discrimination using its color indices, as has been demonstrated with the Johnson system [6]. A review of the potential all-sky calibration star catalogs in the Sloan system and the consequences of transitioning from the Johnson system to the Sloan system on the decades of historical RSO photometry using the Johnson photometric system were discussed in [7]. If the Sloan photometric system does provide discrimination of satellites akin to that of the Johnson photometric system then satellite observations in the Sloan photometric system become an attractive new technology to employ for photometry used for satellite characterization. This is the purpose of the work described in this paper, i.e. we wish to determine if the color

[1] https://www.eso.org/sci/observing/phase2/ObsConditions.html

indices formed with the Sloan filters discriminate between satellites as well as the color indices formed using the Johnson filters.

2. APPROACH

We chose to perform an empirical study of RSO photometric signatures collected in both photometric systems (Johnson-Cousins and Sloan) throughout the course of a night in order to obtain as much phase angle diversity in the measurements as possible. The observations were collected at The Remote Observatory for Variable Object Research (ROVOR). The observatory is located in central Utah at 112°43' 01.0''W, 39°27' 17.1''N and 4579 feet above sea level [8]. The telescope is a 0.4m Ritchey-Chretien optical tube on a German-equatorial Paramount ME pier. The optics have an f/9 focal ratio in an open truss configuration with a primary mirror ion milled to 1/30 wave rms. The camera is an FLI ProLine PL003 with a back-illuminated 1024 × 1024 24 μm pixel SITe detector. The filter wheel is a 12-position FLI Centerline equipped with a set of 50 mm square Astrodon Johnson-Cousins BVRI and Sloan g'r'i'z' filters. The field of view (FOV) is 23.4 arcminutes on a side with a resolution of 1.37''/pixel. Pointing is accurate to better than 30'' within 45 degrees of the zenith.

Four RSOs in geosynchronous orbit were selected for the study. These were chosen for their observability from ROVOR and because they represent various satellite bus types. The description of these satellites is shown in Tab. 1. Given that there are a limited number of space-worthy satellite materials, it is assumed that this set of RSOs samples the material variations adequately enough that this sample size is not biased. Notional artist renderings of the satellites are shown in Fig. 1.[2]

Tab. 1. Description of Geosynchronous satellites observed for this research.

Satellite Descriptions				
Number	**Name**	**Launch Date**	**Bus Type**	**Country**
25740	Nimiq-1	1999-05-20	Lockheed Martin A2100AX	Canada
38342	Nimiq-6	2012-05-17	Loral Space Systems SSL-1300	Canada
37809	SES-2	2011-09-21	Orbital Star-2.4	USA
32018	Spaceway 3	2005-11-16	Boeing BSS-702	USA

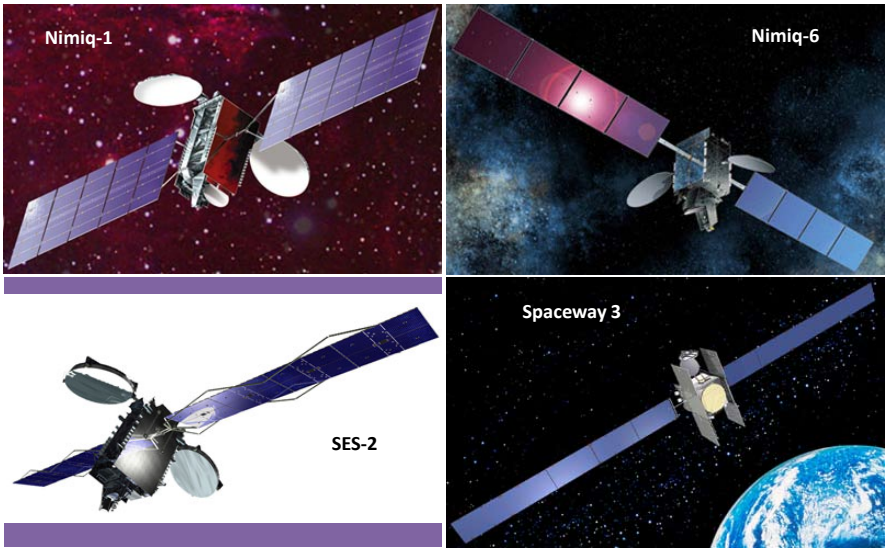

Fig. 1. Notional artist renderings of the four satellites observed for this research.

[2] Internet source: Gunter's Space Page, http://space.skyrocket.de/

3. OBSERVATIONS

On the night of May 11-12, 2016 (i.e. May 12 UT), we successfully observed the satellites NIMIQ-1 (25740), NIMIQ-6 (38342), Spaceway3 (32018), and SES-2 (37809) in the Johnson-Cousins filters B V R I and Sloan g' r' i' z' at each pointing. We observed standard stars SA107-351, SA107-1006, and SA109-381 for calibration purposes. The sequence and details of the observations is given in Tab. 2.

Tab. 2. Basic observational data

Object	Exposure Times (sec)								Comments
	B	V	R	I	g'	r'	i'	z'	
NIMIQ-1 (25740)	6	4	2	3	3	3	3	5	33 pointings 1 frame in each filter, starting at 4:45:20 UT
NIMIQ-6 (38342)	8	6	6	6	6	6	6	6	33 pointings 1 frame in each filter, starting at 4:48:51 UT
Spaceway 3 (32018)	6	4	3	3	3	3	3	5	33 pointings 1 frame in each filter, starting at 4:50:29 UT
SES-2 (37809)	6	4	3	3	3	3	3	5	33 pointings 1 frame in each filter, starting at 4:46:56 UT
SA107-351	60	30	30	30	30	30	30	30	3 pointings of 3 frames in each filter; Mid-point airmasses: 1.96, 1.54, 1.36
SA107-1006	60	30	20	20	30	20	20	30	3 pointings of 3 frames in each filter; Mid-point airmasses: 2.07, 1.59, 1.38
SA109-381	60	30	30	30	30	30	30	30	3 pointings of 3 frames in each filter; Mid-point airmasses: 1.58, 1.41, 1.32

The weather was photometric to the eye and the date of observation was in the middle of a four-day long clear pattern so we expected the results to be accurate and they were. The photometry was extracted from the calibrated image frames using aperture photometry methods. The instrumental magnitude was corrected for extinction via the formula below.

$$v_o = -2.5\log_{10}(\text{counts/sec in V}) + A_v X$$

where v_o is the instrumental magnitude, X is the airmass, and A_v is the extinction coefficient. The above formula is for V explicitly, but the same formula was applied to all the band passes. Extinction coefficients are given in Tab. 3. The error quoted is the standard error, which is the RMS of the values found for the three different stars divided by the square root of the number of stars sampled, which was three.

Tab. 3. Extinction Coefficients, A_x

Filter	Coefficients (magnitudes/airmass)							
	V	B	R	I	g'	r'	i'	z'
Extinction, *A*	0.270	0.155	0.108	0.074	0.231	0.115	0.094	0.088
Error	0.006	0.007	0.006	0.018	0.018	0.013	0.026	0.035

The values of the coefficients for the filter solutions are given in Tab. 4. The internal error is the scatter rms scatter in the value of (standard value – instrumental value) of each star added in quadrature. That is, it is formed with the value of (standard value – instrumental value) for all measurements in a particular filter for each standard star. Then the values are added together for the three stars using the relation:

$$Internal\ Error = \sqrt{\frac{RMS_1^2 + RMS_2^2 + RMS_3^2}{3}}$$

The total error is the deviation between the three stars. It is larger than the internal error because it also includes the uncertainty caused by applying no color correction; that is, the internal error is dominated by the Poisson statistical scatter in the data. The total error is dominated by the differences in the colors of the standard stars. The tabulated coefficients in Tab. 3 and Tab. 4 were used to transform all satellite data into standard magnitudes.

Tab. 4. Standard calibration coefficients

Filter	**Coefficients**							
	B	V	R	I	g'	r'	i'	z'
Zero point ζ (magnitudes)	20.160	20.199	20.379	19.525	20.706	20.460	20.080	19.223
Internal error	0.0051	0.0072	0.0052	0.0058	0.0076	0.0070	0.0059	0.0099
Total error	0.015	0.009	0.010	0.040	0.045	0.035	0.060	0.091

An extinction plot for the standard star SA109-381 is shown in Fig. 2, this shows that the observing conditions throughout the night were stable and photometric. Similar plots for the other two standard stars show the same results. The symbols represent the data and the dotted lines show the linear fit through the data for all eight filters.

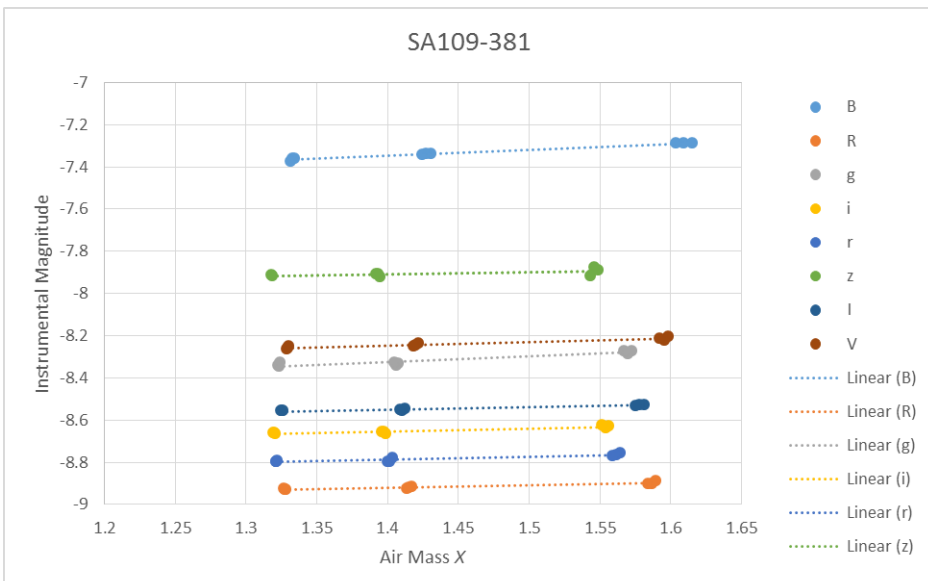

Fig. 2. Extinction plot, instrumental magnitude plotted against airmass for SA109-381.

4. RESULTS

The satellite photometric signatures, color-index signatures, and color-color plots using the Johnson-Cousins and Sloan systems are analyzed first. Then we assess the discrimination capability of each system using the Mahalanobis Distance as the metric. The more tightly clustered each satellite's distribution is in Mahalanobis space and the more separated they are from each other, the better the discrimination capability of the photometric system. The spectral distribution of each photometric system is shown in Fig. 3[3].

[3] From http://www.astrodon.com/index.html

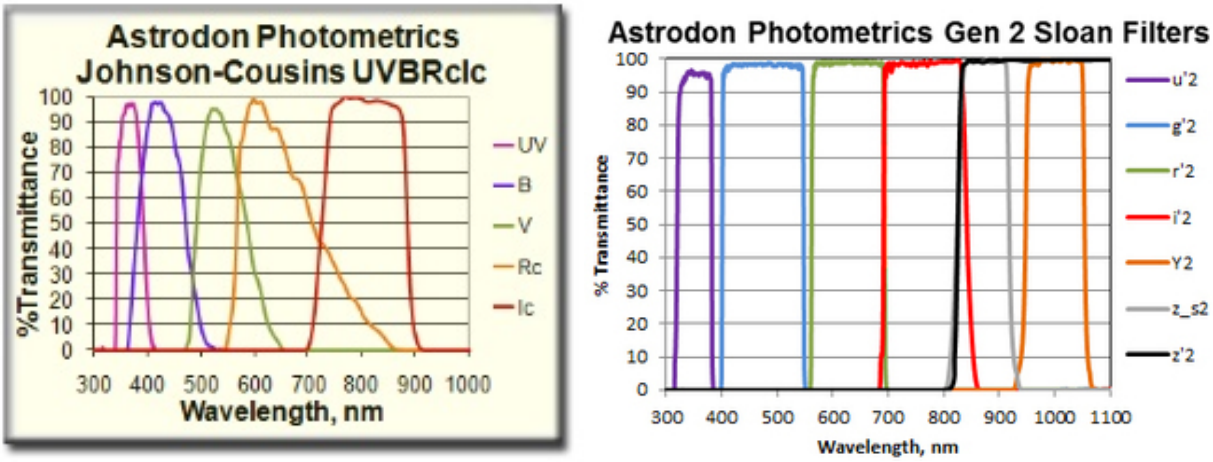

Fig. 3. The spectral properties of the Johnson-Cousins and Sloan photometric systems

4.1 Brightness and Color Comparisons

First we consider the satellite signatures in both systems. Fig. 4 shows the signatures of Nimiq-1. There is a gentle brightening of the satellite between 20 and 40 degrees longitudinal phase angle (LPA). In both systems, the satellite is faintest in the bluer filter (B and g respectively for Johnson-Cousins and Sloan) and brightest in the reddest filter (I and z, respectively). Note that the relative brightness differences between filters in each system are different and that the slopes of the signatures are different for some LPA between the two systems, e.g. between 50 and 80 degrees LPA in Fig. 4. This will be discussed further when we examine the color index signatures.

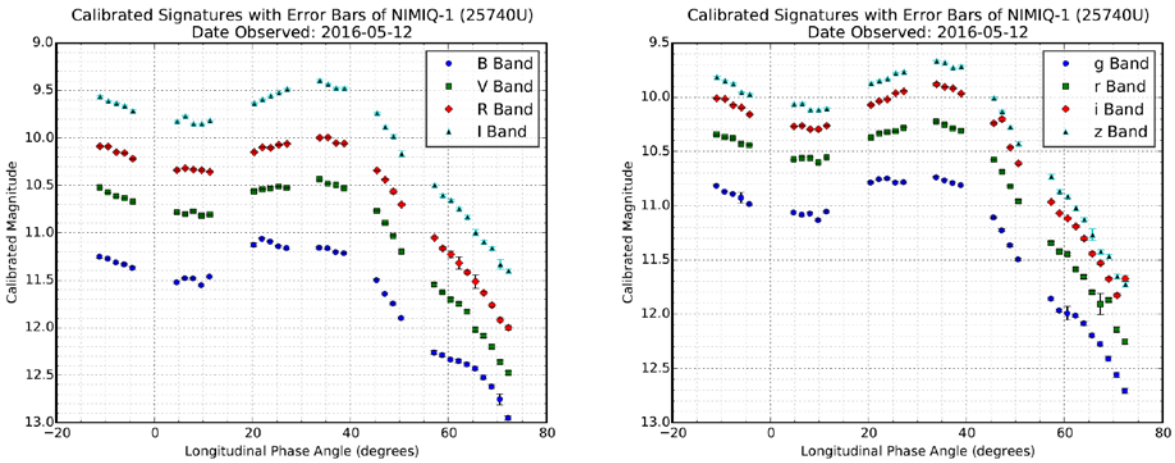

Fig. 4. Photometric signatures of Nimiq-1 in Johnson-Cousins (left) and Sloan (right).

The photometric signatures of Nimiq-6 are shown in Fig. 5. Note that brightness peaks are not detected in either system. There appears to be more brightness variations in the z band signature at large LPA (55 – 70 degrees). Again, in both systems, the satellite is faintest in the bluer filter and brightest in the reddest filter.

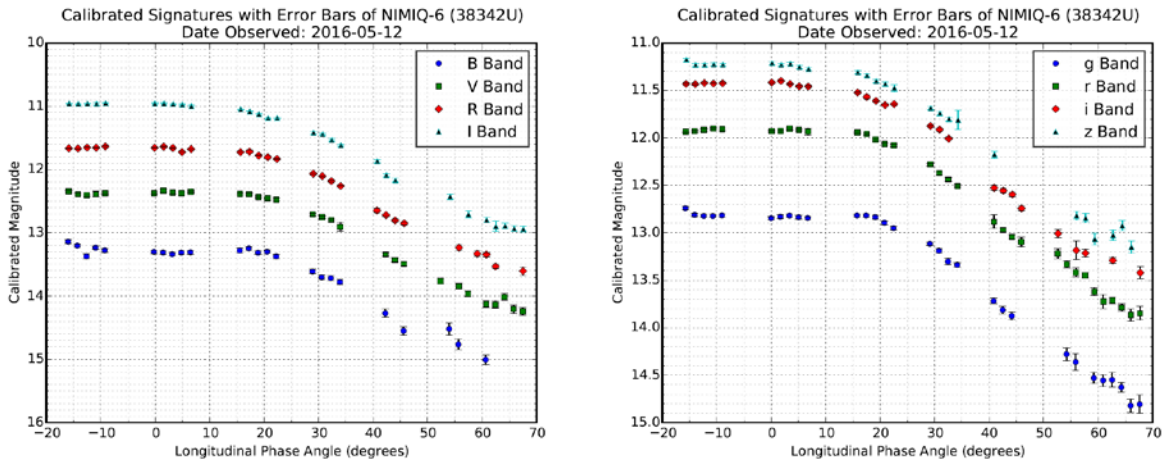

Fig. 5. Photometric signatures of Nimiq-6 in Johnson-Cousins (left) and Sloan (right).

Signatures of SES-2 shown in Fig. 6 show a sharp brightness peak near 5 degrees LPA and a broader brightness peak at 40 degrees LPA. In the Johnson-Cousins system (left), the satellite is brightest in the I band (reddest wavelength) and faintest in the B band (bluest wavelength) but in the Sloan system (right), the satellite is brightest in the i band (the next to the reddest band) with the z and r bands almost the same brightness. So here is the first indication that satellite signatures behave differently when measured in the Sloan system. This satellite is the only one in the four we observed that exhibits this photometric behavior. SES-2 signatures exhibit sharp brightness peaks around zero LPA and a broad brightening around 40 degrees LPA like Nimiq-1 even though their bus types differ, i.e. Boeing 702 and Orbital Star-2.4.

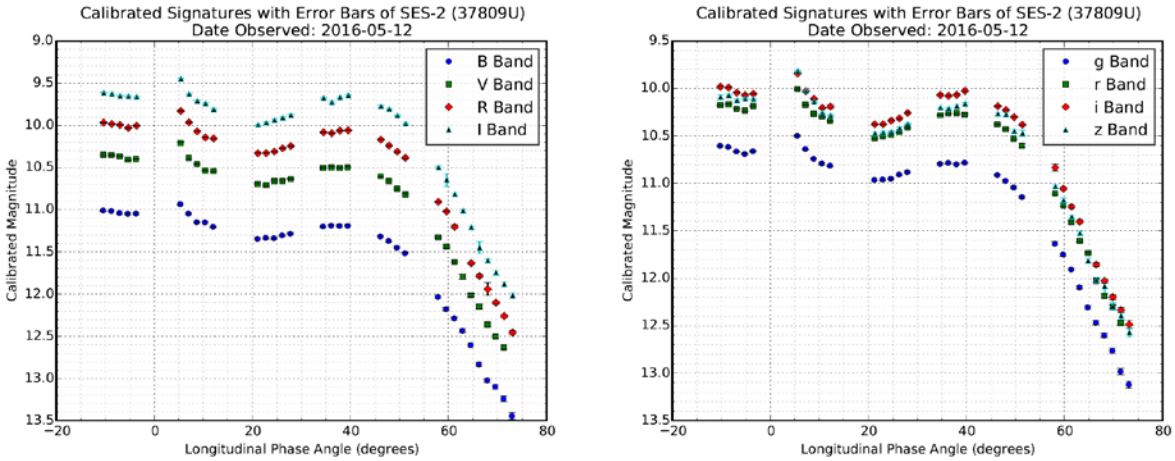

Fig. 6. Photometric signatures of SES-2 in Johnson-Cousins (left) and Sloan (right).

Fig. 7 shows the signatures of Spaceway-3. In this case, the satellite is faintest in the bluer filter and brightest in the reddest filter in both systems. It appears to have a double sharp peak near zero LPA although this is hard to see because of gaps in the collection and another sharp brightness peak at 20 degrees LPA.

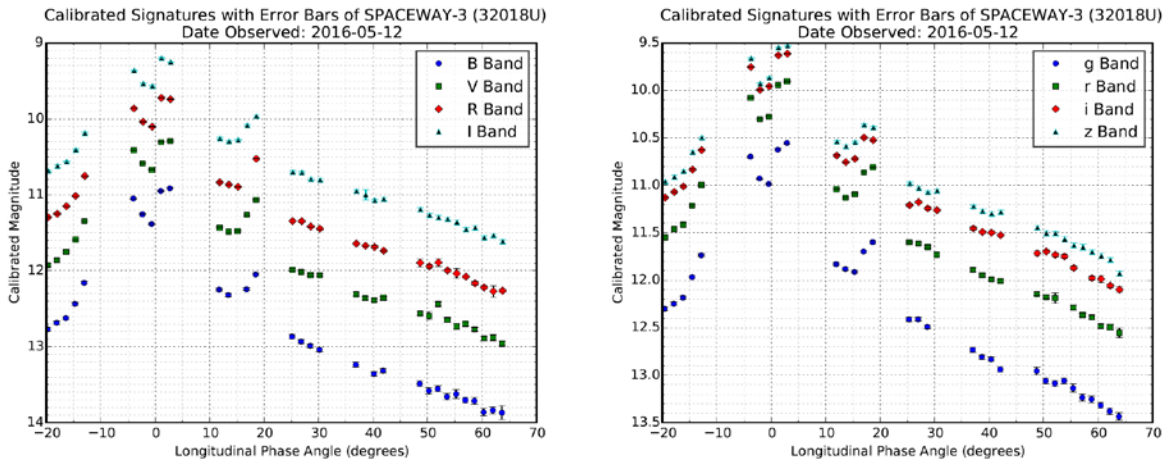

Fig. 7. Photometric signatures of Spaceway-3 in Johnson-Cousins (left) and Sloan (right).

It is useful to visualize the signatures of the different satellites in the same filter to gain insight into how similar or different their brightnesses are with respect to each other in the different bands. Fig. 8 shows the four bands of the Johnson-Cousin system for all four satellites. Note that in all bands, the signatures of Nimiq-1 and SES-2 are close to one another across all LPA. Also note that during glints of Spaceway-3, its brightness tends to become more similar to Nimiq-1 and SES-2. Under all observed LPA, Nimiq-6 is the faintest in all bands.

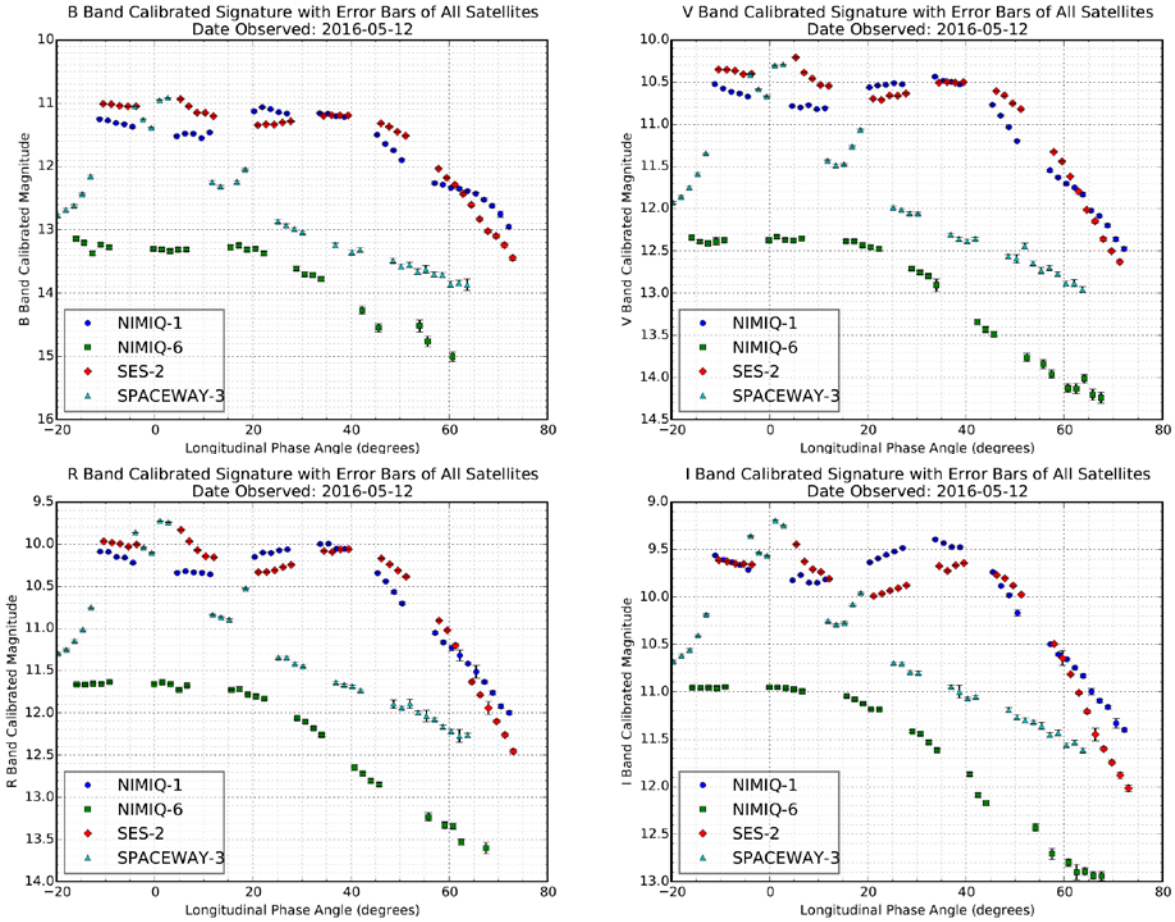

Fig. 8. Comparison of the satellite signatures in each of the Johnson-Cousins filters.

Fig. 9 shows the four bands of the Sloan system for all four satellites. Note that the satellites' photometric signatures exhibit similar behavior as in the Johnson-Cousins system. This is an indication that the Sloan system may have the same discrimination capability as the Johnson-Cousins system. So now we will analyze the color-indices in each system to investigate this further.

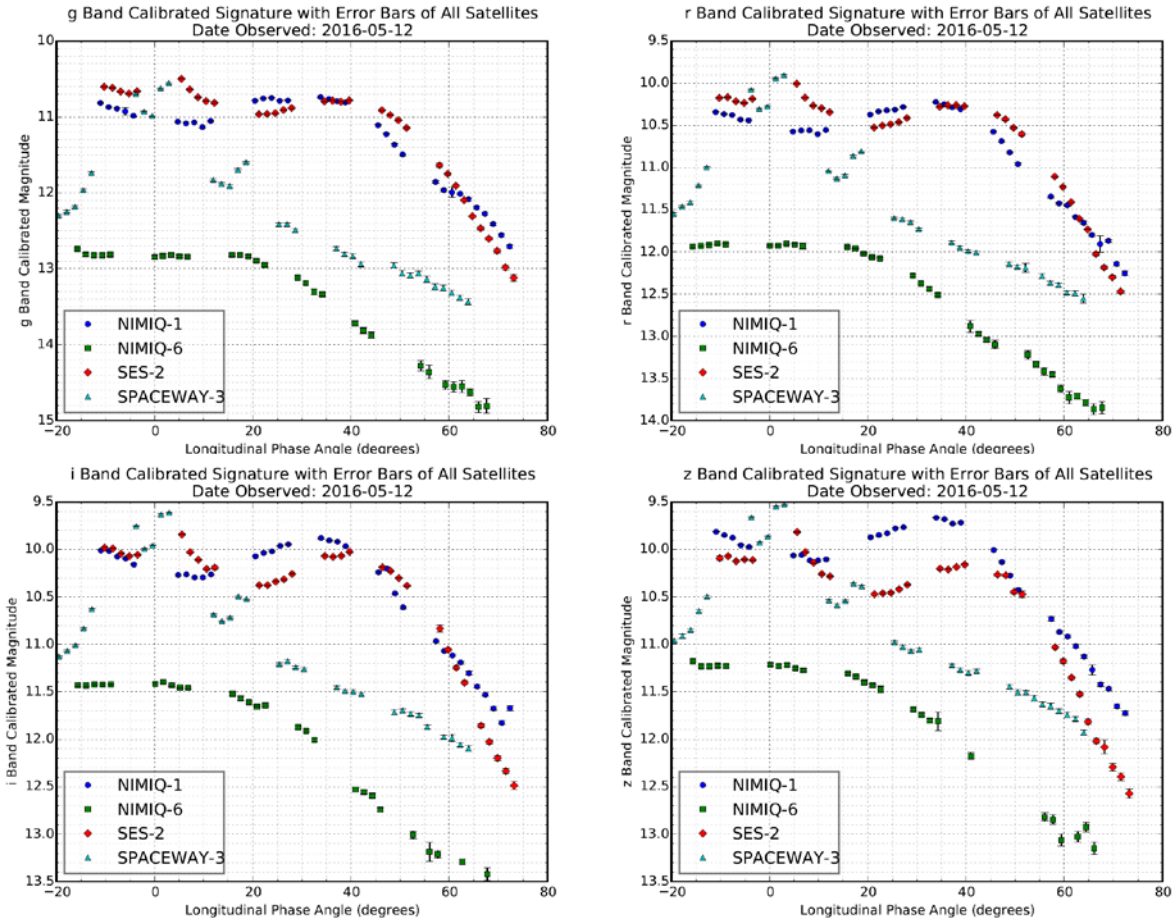

Fig. 9. Comparison of the satellite signatures in each of the Sloan filters.

The photometry from both systems was used to generate color indices that were used in the discrimination analysis. Color indices quantify the ratio of the fluxes in two spectral bands. In a set of four filters, there are six possible filter combinations that are non-degenerate. Tab. 5 shows the combinations for both the Johnson-Cousins and Sloan systems. There are then six unique color-index signatures per photometric system to analyze. For clarity, we discuss the results for what has been found to be the pairs of color indices in each system that produce the greatest separation between satellites and have included the other eight color-index signatures in Appendix A. These are the Johnson-Cousins color indices of B-R and V-I and the Sloan color indices of g-i and r-z. Our analysis showed that these two combinations in each system provide 0.1 magnitude better separation than any other combinations. For each color index we form, the larger the number, the redder the satellite color. The six pairs of non-degenerate color-indices are listed in Tab. 6. We first analyze the color-index signatures in the Johnson-Cousins system.

Tab. 5. Non-degenerate photometric filter combinations for both systems.

Johnson-Cousins	Sloan
B-V	g-r
B-R	g-i
B-I	g-z
V-R	r-i
V-I	r-z
R-I	i-z

Tab. 6. The non-degenerate pairs of color indices used to measure discrimination capability of the photometry systems.

Johnson-Cousins Color Indices	Sloan Color Indices
B-V and R-I	g'-r' and i'-z'
B-R and V-I	g'-i' and r'-z'
B-I and V-R	g'-z' and r'-i'

Fig. 10 shows the satellite B-R signatures along with the mean, median, standard deviation, and median average deviation of the color index across all the observed LPA. Note that Nimiq-1 and SES-2 are of similar B-R colors across all LPA. Spaceway-3's color changes during the glints to be like the former two but otherwise has a similar color as Nimiq-6. Nimiq-6 and Spaceway-3 are also redder than Nimiq-1 and SES-2.

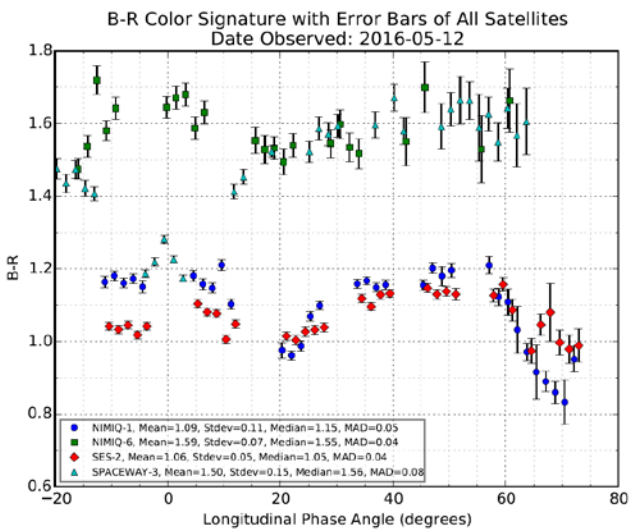

Fig. 10. B-R color index signatures of the four satellites.

In the V-I signatures, Nimiq-1 and SES-2 have more distinct colors from each other (see Fig. 11) than in B-R. Spaceway-3's color again gets bluer during the glint but otherwise it has a similar color as Nimiq-6. Also similar to B-R, Nimiq-6 and Spaceway-3 are redder than Nimiq-1 and SES-2.

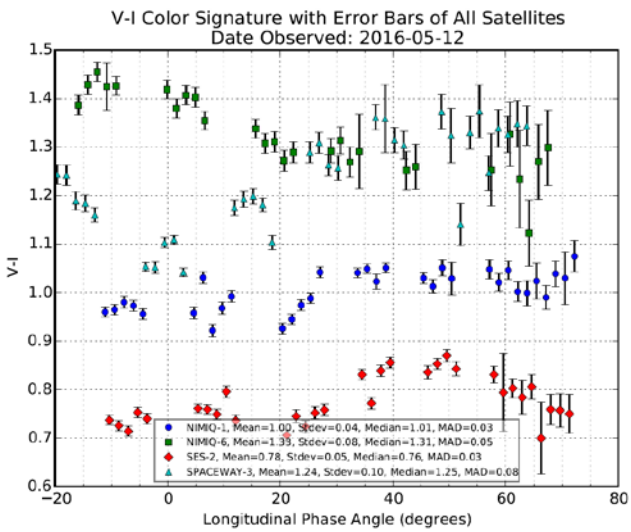

Fig. 11. V-I color index signatures of the four satellites.

Now consider the color-indices in the Sloan system. Fig. 12 shows the satellite signatures in the g-i color index. All four satellites signatures are similar to their B-R signatures (Fig. 10) except that Nimiq-1 and SES-2 are separated further apart in g-i. This is an indication that g-i could provide more discrimination than B-R, at least for these two satellites. However, Nimiq-6 and Spaceway-3 still overlap in g-i like they do in B-R. So we have not gained discriminating power in this case.

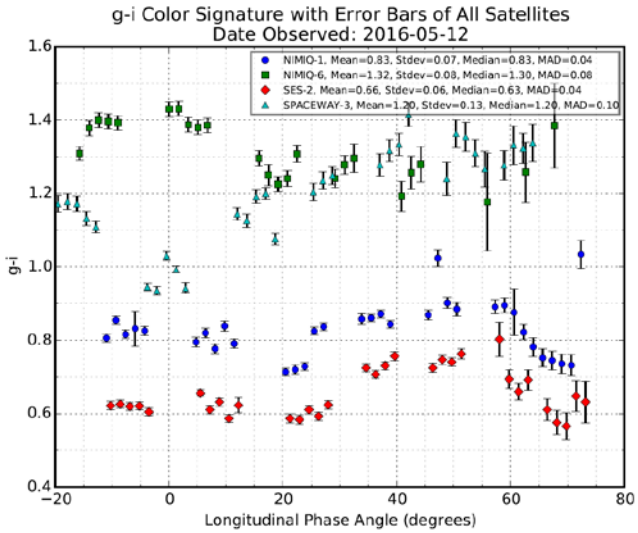

Fig. 12. g-i color index signatures of the four satellites.

In the r-z color index (Fig. 13), the signatures for three of the satellites are similar, which leads one to be concerned that there may be a loss in discrimination power. Since up to this point in the analysis there is ambiguity in whether there is similar or less discrimination in the Sloan system, we now examine the data using color-color diagrams and then will quantify the separation of the satellites in this color-color space in order to definitively determine if the Sloan system is as good as or worse than the Johnson-Cousins system in distinguishing satellites from each other.

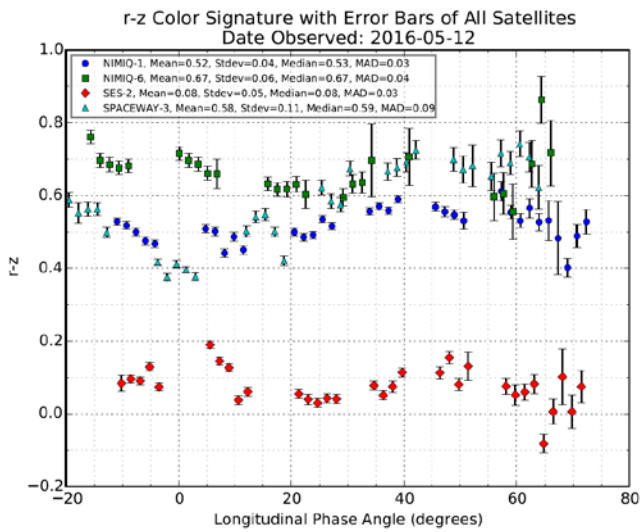

Fig. 13. r-z color index signatures of the four satellites.

There are three non-degenerate pairs of color-indices for each of the four filters in each photometric system. These pairs are shown in Tab. 6 for both the Johnson-Cousins and Sloan systems.

Consider the pairs of color indices B-R and V-I from the Johnson-Cousins system and g-i and r-z from the Sloan system. The other possible color-color plots are shown in Appendix B. Fig. 14 is the color –color diagram for the four satellites in B-R and V-I. Note that the similarities and differences in color signatures are easily discernable using this type of diagram. The satellites with the same colors in both bands cluster on top of one another (Nimiq-6 and Spaceway-3). Although Nimiq-1 and SES-2 have similar B-R colors, their V-I colors are different and therefore their clusters are close but not overlapping. So by eye and with computational methods, the satellites that separate in this diagram can be distinguished from one another and uniquely identified.

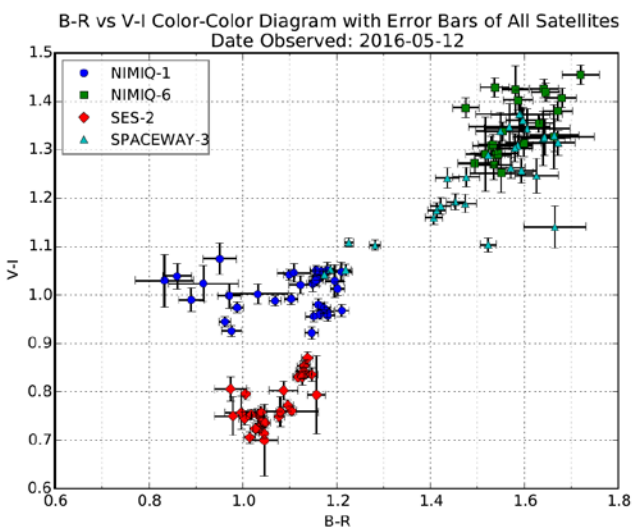

Fig. 14. Color-color diagram using B-R and V-I in the Johnson-Cousins system

Fig. 15 is the color –color diagram for the four satellites in g-i and r-z. Note the similar clustering as in Fig. 14. Nimiq-1 and SES-2 are slightly more separated but Nimiq-6 and Spaceway-3 still lie on top of one another in this space. In both photometric systems, Spaceway-3 gets bluer during its glints (as seen in the signature plots above). Therefore, these diagrams indicate that although we do not gain discrimination power, we also do not appear to lose any by using the Sloan system. We will verify this result in the next section by calculating the Mahalanobis Distance of each satellite distribution in color-color space for both systems.

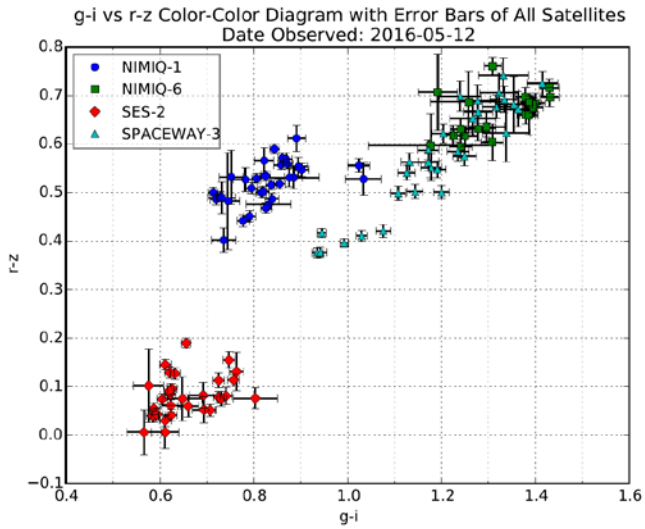

Fig. 15. Color-color diagram using g-i and r-z in the Sloan system

4.2 Discrimination Analysis

The Mahalanobis Distance is used in multi-dimensional statistical analysis for testing hypotheses and classification of observations. It was originally used as a distance between two normal distributions with expectations μ_1 and μ_2 and common covariance matrix Σ. Here Mahalanobis Distance is defined as:

$$D_M(\vec{x}) = \sqrt{(\vec{x} - \vec{\mu})^T S^{-1} (\vec{x} - \vec{\mu})}$$

Where $\vec{x} = (x_1, \dots, x_n)^T$ is a set of observations with mean $\vec{\mu} = (\mu, \dots, \mu_n)^T$ and covariance matrix S.[4] If the covariance matrix is the identity matrix, then the Mahalanobis Distance reduces to the Euclidean Distance. Mahalanobis Distance is a useful metric for distributions that are not spherically symmetric in the parameter space. The Mahalanobis Distance is the distance of a test point from the center of mass of the data distribution divided by the width of the ellipsoid in the direction of the test point.

To perform the analysis, we use the "leave one out" method. This allows us to use each observation in turn as the test point to compare it with the rest of the observations making up the distribution. This is done for the color-color pairs discussed above for each system. Then the results for each satellite are compared. In some cases in Fig. 16, Sloan shows slightly better clustering (e.g. Nimiq-1), whereas in other cases, Johnson-Cousins shows slightly better clustering (e.g. Spaceway-3). But overall, there is no real significant difference in the distributions formed in both systems. This means that the two photometric systems yield similar discrimination results between the satellites.

[4] From https://en.wikipedia.org/wiki/Mahalanobis_distance

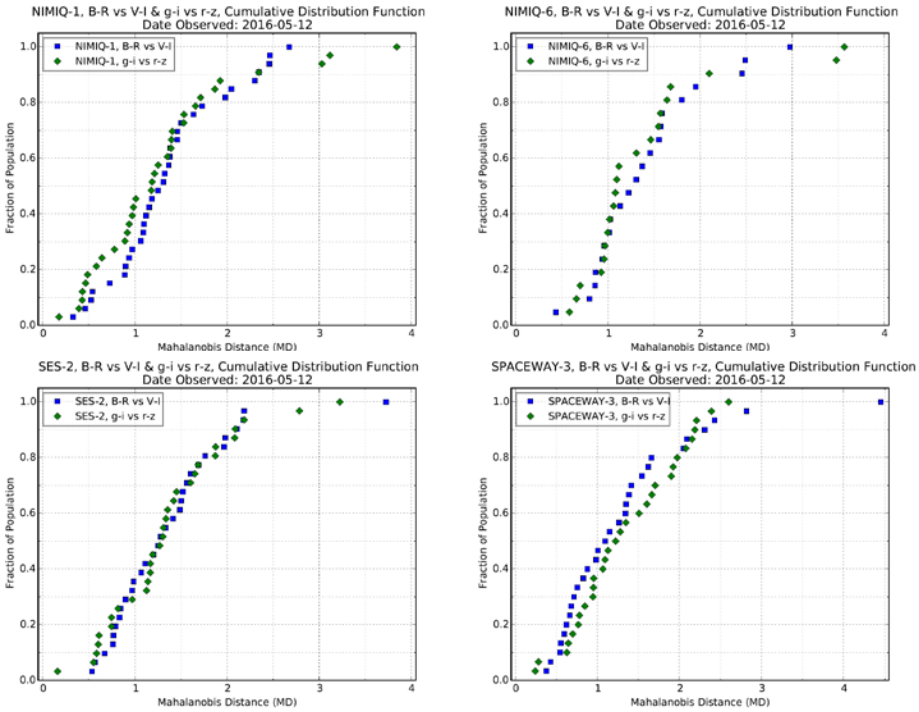

Fig. 16. A comparison of the cumulative distribution functions of the color index pairs formed using the Johnson-Cousins system and the Sloan system.

5. CONCLUSIONS

Using photometric observations collected on four RSOs in geosynchronous orbit with both Johnson-Cousins BRVI and Sloan g'r'i'z' filters, we have shown that the Sloan system performs as well as the Johnson-Cousin system in discriminating satellites from each other based on their spectral photometric properties. Although the observations spanned a large range of longitudinal phase angle, the sample of satellites was small and limited to one night, therefore only sampling one solar declination. These limitations add uncertainty to our conclusion. Let us discuss each deficiency separately. Because there are a small number of space-worthy satellite materials and satellite configurations, we argue that the sample of four spans the variations in these parameters adequately, although a study using more satellites that sample all the different bus types used in geosynchronous orbit would confirm these results. Because we have studied the photometric signatures of over a hundred RSOs in geosynchronous orbit spanning two decades, based on this experience, we find these signatures sufficiently represent the range of possible signatures to form the basis of our conclusion. To underscore this, we point out that the signatures do contain glints and therefore the observations do sample a sufficient amount of variability. Future work collecting more satellite signatures using the Sloan filters is desirable. Experiments with in-frame photometric calibrations while collecting these signatures would be useful as a proof of concept.

6. REFERENCES

1. M. Fukugita, T. Ichikawa, J. E. Gunn, M. Doi, K. Shimasaku and D. P. Schneider, "The Sloan Digital Sky Survey Photometric System," *The Astronomical Journal* , vol. 111, pp. 1748-1756, 1996.
2 D. G. York, J. Adelman, J. E. Anderson Jr., S. F. Anderson, J. Annis, N. A. Bahcall, J. A. Bakken, R. Barkhouser, S. Bastian, E. Berman, W. N. Boroski, S. Bracker, C. Briegel and J. W. Briggs, "The Sloan Digital Sky Survey: Technical Summary," *The Astronomical Journal*, vol. 120, pp. 1579-1587, 2000.
3 K. N. Abazajian, J. K. Adelman-McCarthy, M. A. Agueros, S. S. Allam, C. A. Prieto, D. An, K. S. J. Anderson, S. F. Anderson, J. Annis, N. A. Bahcall, C. A. L. Bailer-Jones and J. C. Barentine, "The Seventh Data Release of the Sloan Digital Sky Survey," *The Astrophysical Journal Supplement Series*, vol. 182, pp. 543-558, 2009.
4 J. L. Tonry, C. W. Stubbs, K. R. Lykke, P. Doherty, I. S. Shivvers, W. S. Burgett, K. C. Chambers, K. W. Hodapp, N. Kaiser, R. P. Kudritzki, E. A. Magnier, J. S. Morgan, P. A. Price and R. J. Wainscoat, "The Pan-STARRS1 Photometric System," *The Astrophysical Journal*, vol. 750, p. 99, 2012.

5 E. A. Magnier, E. Schlafly, D. Finkbeiner, M. Juric, J. L. Tonry, W. S. Burgett, K. C. Chambers, H. A. Flewelling, N. Kaiser, R. P. Kudritzki, J. S. Morgan, P. A. Price, W. E. Sweeney and C. W. Stubbs, "The Pan-STARRS 1 Photometric Reference Ladder, Release 12.01," *The Astrophysical Journal Supplement Series*, vol. 205, p. 20, 2013.
6 T. E. Payne, S. A. Gregory, D. J. Sanchez, L. G. Finkner, D. M. Payne, L. Kann, C. K. Davis and D. Werling, "Space Object Identification of Geosynchronous Satellites," in *AMOS Technical Conference*, 1999.
7 Payne, T.E., Castro, P.J., Gregory, S.A., Dao, P., "Satellite Photometric Error Determination", AMOS Conference Proceedings, September 2015.
8 Moody, J. W., Boizelle, B., Bates, K., Little, B., McCombs, T., Nelson, J., Pace, C., Pearson, R. L. III, Harrison, J., Brown, P. J., and Barnes, J. "Remote Observatory for Variable Object Research (ROVOR)", *PASP*, **124** (919), 956-962, 2012.

7. APPENDIX A: COLOR SIGNATURES

This appendix contains the satellite signatures using the other possible color indices; namely B-V, B-I, B-R, and R-I in the Johnson-Cousins system and g-r, g-z, r-i, and i-z in the Sloan System.

7.1 Johnson-Cousin Color Index Signatures

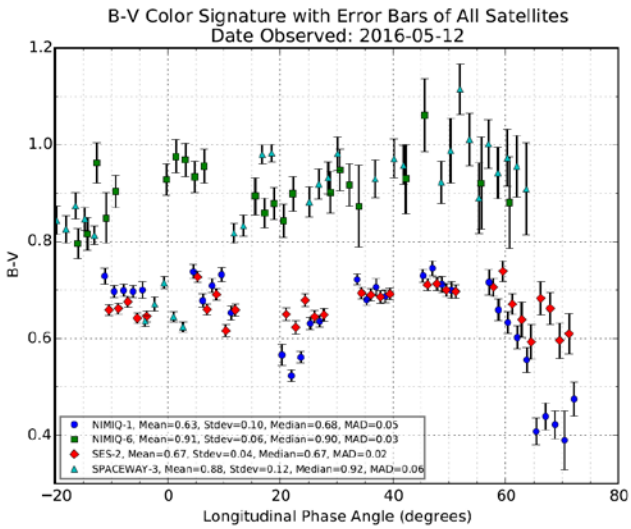

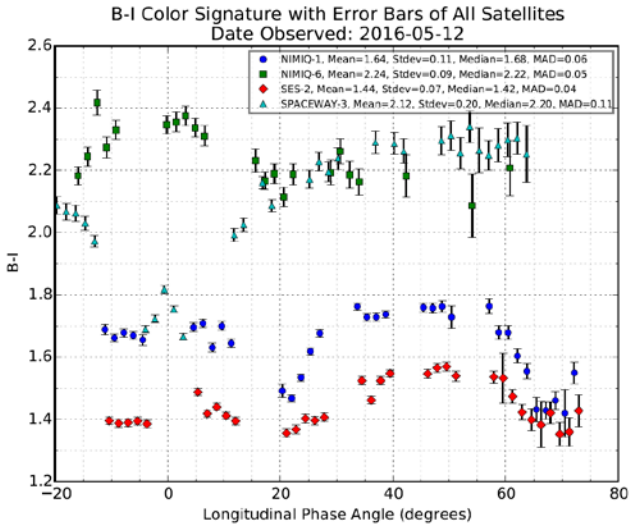

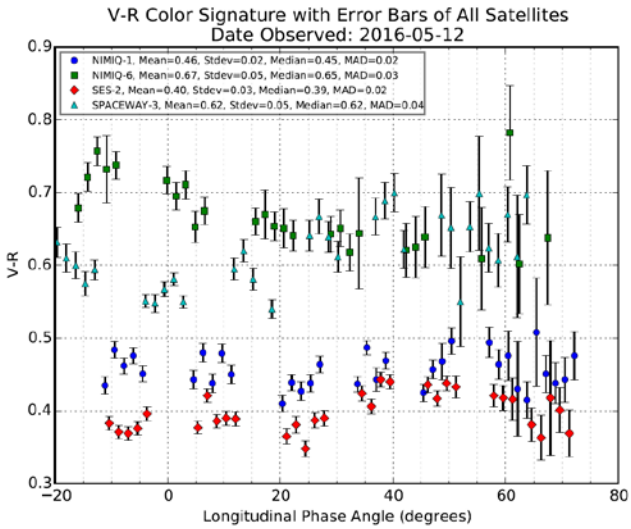

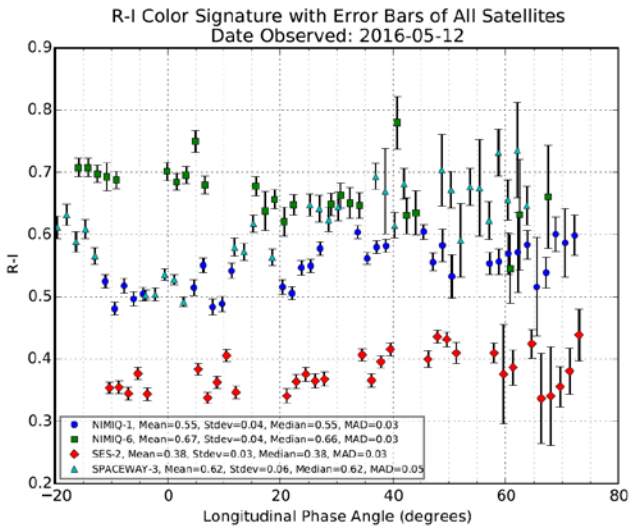

7.2 Sloan Color Index Signatures

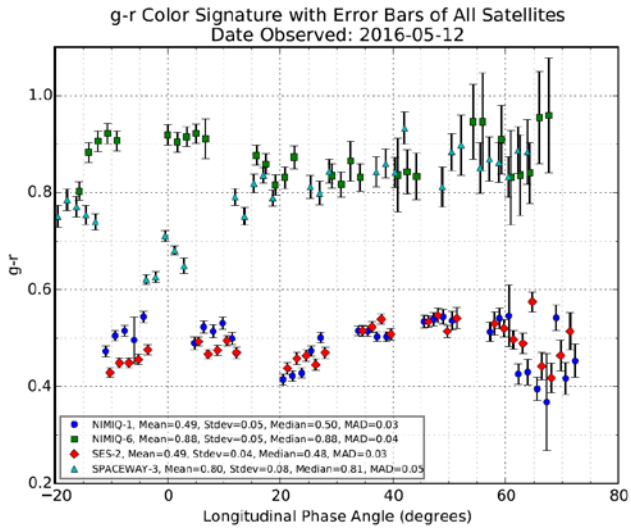

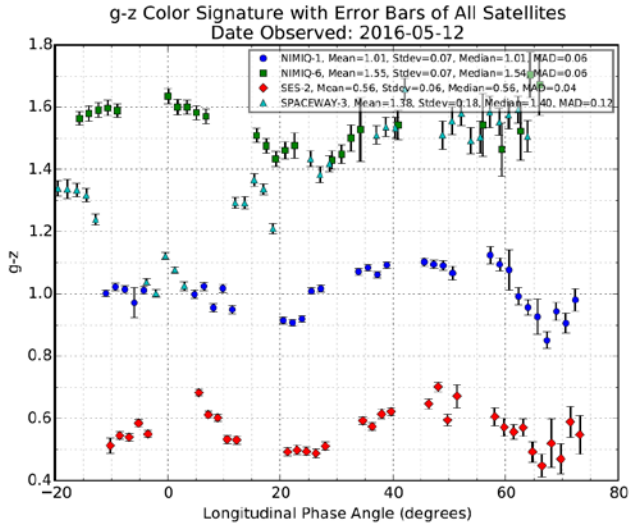

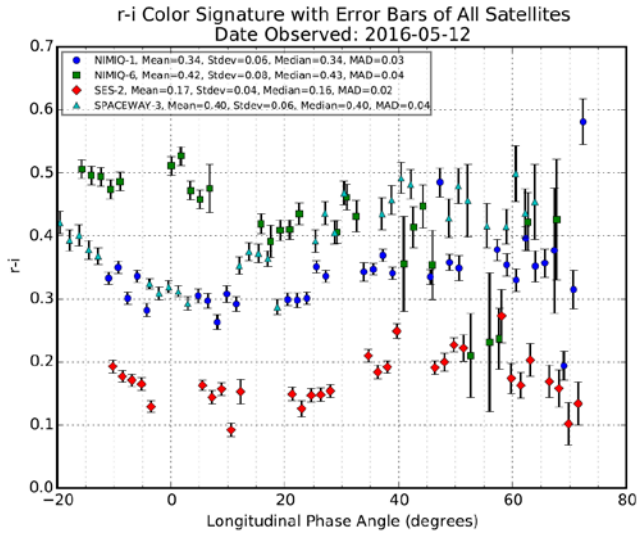

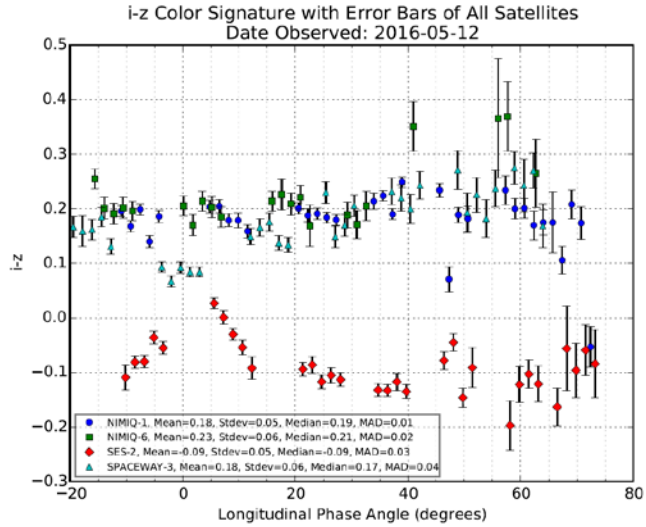

8. APPENDIX B: COLOR-COLOR DIAGRAMS

This appendix contains the color-color diagrams using the other possible color index pairs; namely B-V and R-I, and B-I and V-R in the Johnson-Cousins system and g-r and i-z, and g-z and r-i in the Sloan System.

8.1 Johnson-Cousin Color-Color Diagrams

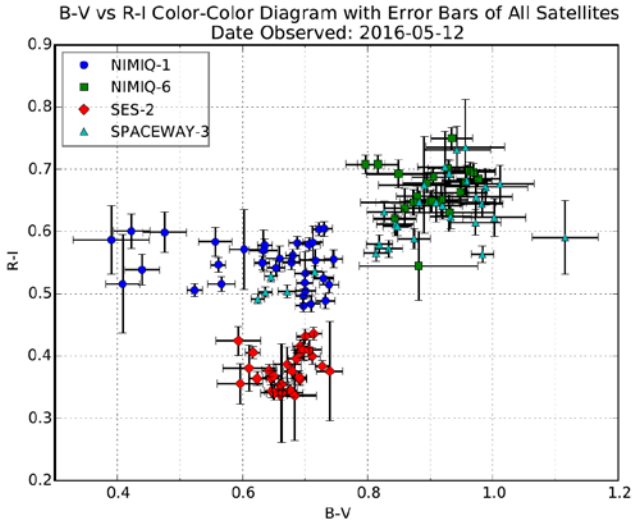

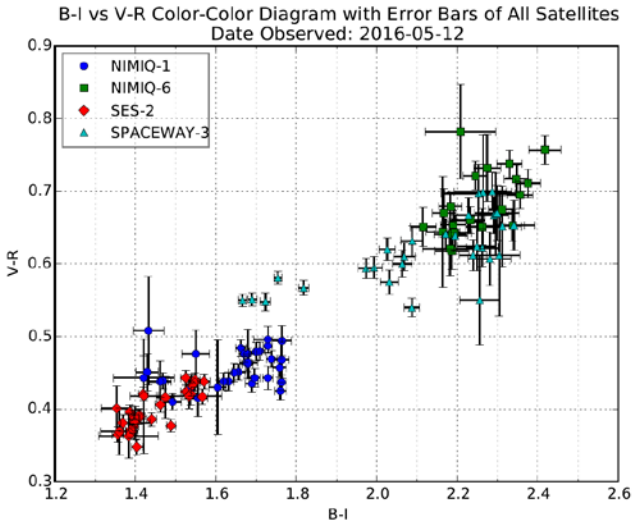

8.2 Sloan Color-Color Diagrams